Proc. Natl. Acad. Sci. USA
Vol. 90, pp. 1–5, January 1993
Biochemistry

Perturbation of the secondary structure of the scrapie prion protein under conditions that alter infectivity

(β-sheets/amyloid/liposomes/denaturation/attenuated total reflection–Fourier transform infrared spectroscopy)

MARÍA GASSET*, MICHAEL A. BALDWIN*, ROBERT J. FLETTERICK†‡, AND STANLEY B. PRUSINER*‡§

Departments of *Neurology, †Pharmaceutical Chemistry, and ‡Biochemistry and Biophysics, University of California, San Francisco, CA 94143

Contributed by Stanley B. Prusiner, August 17, 1992

ABSTRACT **Limited proteolysis of the scrapie prion protein (PrP^{Sc}) generates PrP 27-30, which polymerizes into amyloid. By attenuated total reflection–Fourier transform infrared spectroscopy, PrP 27-30 polymers contained 54% β-sheet, 25% α-helix, 10% turns, and 11% random coil; dispersion into detergent–lipid–protein-complexes preserved infectivity and secondary structure. Almost 60% of the β-sheet was low-frequency infrared-absorbing, reflecting intermolecular aggregation. Decreased low-frequency β-sheet and increased turn content were found after SDS/PAGE, which disassembled the amyloid polymers, denatured PrP 27-30, and diminished scrapie infectivity. Acid-induced transitions were reversible, whereas alkali produced an irreversible transition centered at pH 10 under conditions that diminished infectivity. Whether PrP^{Sc} synthesis involves a transition in the secondary structure of one or more domains of the cellular prion protein from α-helical, random coil, or turn into β-sheet remains to be established.**

Scrapie and related neurodegenerative disorders of humans (1) are caused by prions, which are composed largely, if not entirely, of an abnormal isoform of the prion protein (PrP), designated PrP^{Sc} (2). PrP^{Sc} is derived from the cellular prion protein (PrP^{C}) by a posttranslational process which probably occurs in the endocytic pathway (3–5). Properties of PrP^{Sc} that distinguish it from PrP^{C} are protease resistance, insolubility (6), poor antigenicity (7, 8), resistance to release from membranes by phosphatidylinositol-specific phospholipase C digestion (9), and polymerization of an N-terminally truncated form (PrP 27-30) into amyloid (10, 11).

Enriching fractions for scrapie infectivity led to the discovery of PrP 27-30 (12, 13), which formed rod-shaped amyloid polymers (10). Ultrastructural and histochemical studies showed that prion rods were indistinguishable from the filaments that comprise PrP amyloid plaques (6, 10, 14). Some investigators argue that the prion rods should be designated scrapie-associated fibrils even though the ultrastructural criteria used to define these fibrils clearly distinguished them from amyloid (15, 16). All amyloids studied to date have high β-sheet content and exhibit green-gold birefringence under polarization microscopy after staining with Congo red dye (17, 18). Thus, PrP 27-30 was thought to contain an extensive β-pleated-sheet structure (10).

Since both PrP^{Sc} and PrP^{C} undergo similar posttranslational chemical modifications, the conversion of PrP^{C} into PrP^{Sc} may involve changes only in secondary and tertiary structure. Analysis of the PrP sequence identified several putative structural motifs while tertiary structure modeling of the full-length molecule predicted an N-terminal coil–turn region and a highly structured globular domain (19), the latter corresponding to PrP 27-30.

The publication costs of this article were defrayed in part by page charge payment. This article must therefore be hereby marked "*advertisement*" in accordance with 18 U.S.C. §1734 solely to indicate this fact.

Investigations of the conformation of PrP^{Sc} by conventional spectroscopic techniques have been hampered by its insolubility and the need for substantial amounts of highly purified protein. Algorithms that correlate regions of the infrared (IR) spectrum with the secondary structure of proteins have made Fourier transform infrared (FTIR) spectroscopy a valuable technique for conformational studies, capitalizing on the sensitivity of the stretching vibrations of protein groups to their structural environment. Attenuated total reflection (ATR)–FTIR spectroscopy has a major advantage over the conventional transmission mode for insoluble samples because the analyte is manipulated as a thin hydrated film (20). The amide I band (or amide I′ band for samples in ^2H_2O) at 1700–1600 cm^{-1} is due primarily to the carbonyl stretching vibration, which is sensitive to hydrogen bonding. While the studies reported here were in progress, other investigators reported their findings on transmission FTIR spectroscopy of prion rods sonicated in phosphate-buffered saline (21); these data showed less α-helix and turn but more β-sheet and coil than were predicted theoretically (22).

We report here that PrP 27-30 in prion rods has a high content of β-sheet, as expected for amyloid proteins. Denaturation of PrP 27-30 under conditions leading to a loss of scrapie infectivity (10, 23) reduced β-sheet structure. Whether further investigations will show that the apparent correlation between PrP^{Sc} secondary structure and scrapie infectivity is constant and that "infectivity" is a consequence of the conversion of α-helices, random coils, or turns within PrP^{C} into the β-sheets of PrP^{Sc} is uncertain.

MATERIALS AND METHODS

Materials. Phospholipids were purchased from Avanti Polar Lipids, deuterium oxide from Aldrich, nondenaturing detergents from Calbiochem, SDS from BDH, proteinase K from Beckman, and phenylmethylsulfonyl fluoride from Sigma.

Purification of Scrapie Prions. Purification of PrP 27-30 from scrapie-infected hamster brains has been described (10). From fractions sedimenting in 48–60% (wt/vol) sucrose, prion rods were diluted in distilled water (20% final concentration of sucrose) and centrifuged at 100,000 × *g* for 6 hr. The pellet was resuspended in water, centrifuged again, and then washed twice with chilled ethanol and once with water to remove detergents added during purification. After SDS/PAGE (24), the SDS was removed by three precipitations

Abbreviations: PrP, prion protein; PrP^{Sc}, scrapie isoform of the prion protein; PrP^{C}, cellular isoform of the prion protein; FTIR, Fourier transform infrared; ATR, attenuated total reflection; DLPC, detergent–lipid–protein complex; LF, low-frequency.

§To whom reprint requests should be addressed at: Department of Neurology, HSE-781, University of California, San Francisco, CA 94143-0518.

with 20 volumes of chilled ethanol at −80°C for 3 hr or at −20°C overnight.

IR Spectroscopy. ATR–FTIR spectra were obtained with a Laser Precision Analytical (Yorkville, NY) model RFX-30 FTIR spectrophotometer (25). Proteins (50–100 μg) were dried on the surface of the ATR plate under N_2 at room temperature. Hydrogen/deuterium exchange was achieved by rehydration in ^2H_2O overnight or by flushing ^2H_2O-saturated N_2 over the ATR plate for 2 hr. Fourier self-deconvolution was applied to increase the spectral resolution in the amide I′ region (1700–1600 cm^{-1}). Quantification of the different components used least-squares iterative curve fitting to Lorentzian line shapes. The proportion of each structure of PrP 27-30 was computed from the sum of the areas of all fitted bands having maxima in the appropriate frequency region, normalized for the areas of all bands with maxima between 1689 cm^{-1} and 1615 cm^{-1}. The frequency regions characterizing the different protein structures are as follows: 1662–1645 cm^{-1}, α-helix; 1689–1682 cm^{-1} and 1637–1613 cm^{-1}, β-sheet; 1644.5–1637 cm^{-1}, coil; and 1682–1662.5 cm^{-1}, turns (20).

PrP 27-30 Solubility. The solubility was determined by preparing prion rods in 10 mM phosphate buffer at various pH values. Samples were left at room temperature for 30 min, then centrifuged at 100,000 × *g* for 1 hr. The supernatants were neutralized and normalized to equal salt concentrations, and protein was precipitated with chilled ethanol. The pellets were washed once with water. Fractions were hydrolyzed at 110°C overnight under vacuum with 6 M HCl (Pierce) and phenol (26), and amino acid analysis of the hydrolysate was performed (27). Protein was estimated from the Asx, Glx, Ser, His, and Ile content.

Secondary Structure Prediction. Secondary structure was predicted using EuGene version 3.2 software. Algorithms (22) were used with a window span of 17 residues, with no restriction in the decision constants.

Proteinase K Digestions. PrP 27-30 (10 μg) was digested in 25 μl of 50 mM Tris·HCl (pH 8.0) containing 0.1 M NaCl and 0.1% octyl β-D-glycopyranoside for 1 hr at 37°C (proteinase K/PrP 27-30 weight ratios of 1:50 and 1:30). Digestions were terminated with phenylmethylsulfonyl fluoride. The degree of hydrolysis was determined by SDS/PAGE followed by silver staining, with prion rods as controls.

RESULTS

Secondary Structure of PrP 27-30 in Prion Rods. The ATR–FTIR spectrum of sucrose gradient-purified prion rods in 10 mM phosphate buffer at pH 7.0 is shown in Fig. 1, for the frequency region 1700–1520 cm^{-1} (dotted-line spectrum A). The amide I and II bands are centered at 1640 and 1550 cm^{-1}, respectively. After deuteration the 1700–1600 cm^{-1} band is referred to as amide I′. Deuteration reduced the absorption intensity at 1550 cm^{-1}, the spectrum remaining unchanged after 1 hr of deuteration (solid-line spectrum A). Amide II components unaffected by deuteration indicate highly compact regions of the molecule not accessible to hydrogen exchange. The conformation-sensitive amide I′ band (1700–1600 cm^{-1}) exhibited a maximum at 1625 cm^{-1} and a shoulder at ≈1658 cm^{-1}. We used the absorbance ratio A_{1630}/A_{1660} as an indication of the relative amounts of β-sheet and α-helix, these purified fractions giving a value of 1.35 ± 0.03 (n = 10). The amide I′ band for the prion rods is a composite of several overlapping peaks attributable to a number of components. Fourier self-deconvolution and curve fitting of the solid-line spectrum A in Fig. 1 showed a major component at 1621.5 cm^{-1}, characteristic of aggregated β-sheet structures maintained by hydrogen bonding (Fig. 2*A*). The contributions of the various secondary structural elements are given in Table 1, row A.

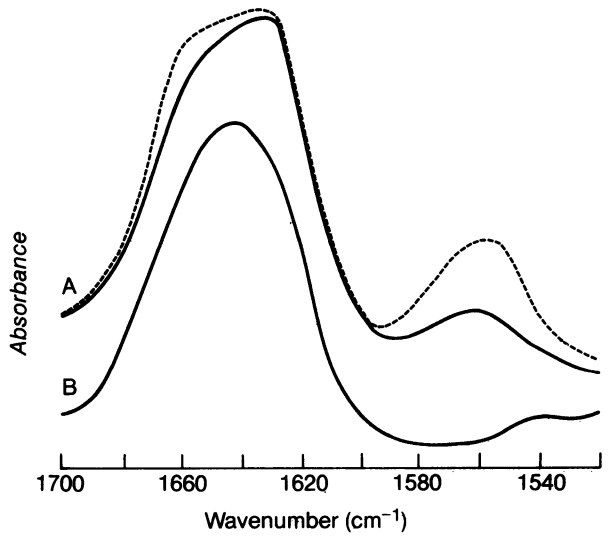

FIG. 1. ATR–FTIR spectra. (Spectra A) Prion rods in 10 mM phosphate buffer (pH 7.4) before (dotted line) and after (solid line) deuteration for 1 hr. (Spectrum B) PrP 27-30 purified by SDS/PAGE and further extensive removal of SDS, prepared in 10 mM phosphate buffer (pH 7.4) after deuteration for 1 hr. Hydrogen (protium deuterium) exchange was required in order to discriminate between α-helix and random coil.

Corrections were evaluated for contributions from other groups in the PrP 27-30 molecule that absorb at 1700–1600 cm^{-1}, including side chains of Arg, Tyr, Gln, and Asn residues, on the basis of the translated PrP gene sequence from Gly-90 to Ser-231 and 12 *N*-acetylglucosamine moieties per molecule (24). The corrections were made by digital subtraction (28) after confirmation of the isotropic nature of the non-peptide amide I′ band-absorbing linkages. The cor-

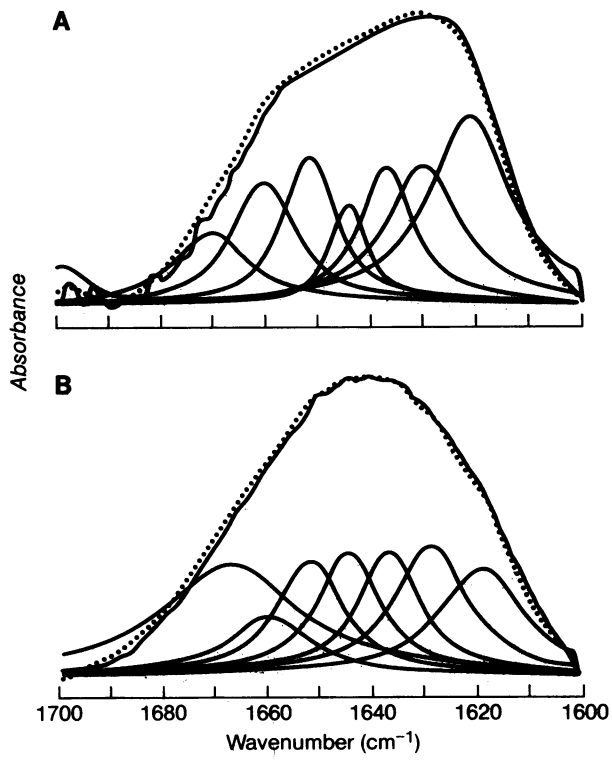

FIG. 2. Curve fitting of the amide I′ region of PrP 27-30 as prion rods (*A*) and PrP 27-30 purified by SDS/PAGE (*B*). The result of the fitting appears under the curve, and the sum of the components is represented by the dotted line.

Table 1. Percentages of secondary structure in PrP 27-30

		% secondary structure (mean ± SD)				
	n	Total β-sheet	LF β-sheet	α-helix	Turns	Coil
(A) Sucrose gradient	10	54.2 ± 4.5	33.4 ± 3.8	24.8 ± 1.7	9.8 ± 1.8	11.2 ± 3.2
(B) Dispersed in lipids	6	50.3 ± 3.2	30.7 ± 1.1	26.4 ± 0.9	11.6 ± 2.1	11.7 ± 1.5
(C) SDS/PAGE	3	38.0 ± 2.0	9.6 ± 1.0	19.3 ± 1.3	29.5 ± 1.7	13.1 ± 1.0
(D) pH 2	3	43.3 ± 2.3	27.7 ± 2.3	22.7 ± 1.8	18.4 ± 1.4	15.6 ± 4.6
(E) pH 12	4	39.0 ± 3.9	26.3 ± 3.8	30.0 ± 2.5	21.3 ± 4.9	9.7 ± 2.5
(F) Predicted	—	37	—	30	19	14

Rows: A, isolated by zonal centrifugation in 48–60% sucrose; B, dispersed in dimyristoyl DL-α-phosphatidylcholine; C, purified by SDS/PAGE followed by removal of SDS; D, at pH 2; E, at pH 12; F, predicted (22). *n*, No. of samples; LF, low-frequency.

rected contributions of the various structural elements changed little from the data in Table 1, row A; thus, only uncorrected values are given. Comparison of the experimentally determined proportions of the various structural features (Table 1, row A) with the Garnier *et al.* (22) predictions (Table 1, row F) revealed that PrP 27-30 has significantly more β-sheet than predicted, and less turn.

Dispersion of the Prion Rods into Detergent–Lipid–Protein Complexes (DLPCs). Octyl β-D-glucopyranoside (0.1–1.0%, wt/wt) (Fig. 3, spectrum A), as well as *n*-octyl maltoside, *n*-dodecyl glucoside, *n*-dodecyl maltoside, Zwittergent 3-14, and Triton X-100 (data not shown), did not modify the amide I′ band lineshape. Dispersion of prion rods into DLPCs (29) increased the IR absorption efficiency, probably by orienting the protein molecules and improving the contact with the germanium crystal. This effect was greatest for phospholipids with short, saturated acyl chains, perhaps by increasing the number of layers that the IR radiation penetrated. Polarized ATR revealed that the predominant orientation of PrP 27-30 molecules was parallel to the germanium crystal (data not shown), but there was no preferential orientation of any particular secondary structural element. No substantive change in the secondary structure of PrP 27-30 appeared to occur during DLPC formation (Table 1, row B); ATR–FTIR spectra of PrP 27-30 were independent of the phospholipid headgroup (phosphatidylcholine vs. phosphatidylglycerol; Fig. 3, spectra C and D vs. spectra E and F) and chain length and degree of saturation (dimyristoyl vs. dioleoyl; Fig. 3, spectra C and E vs. spectra D and F).

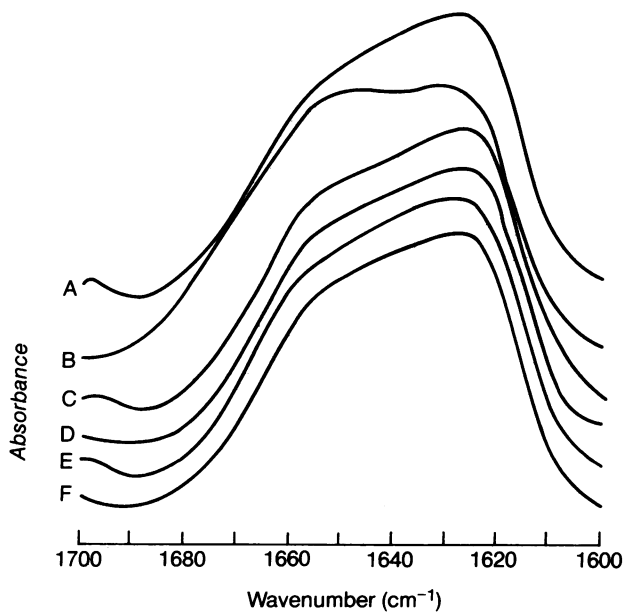

FIG. 3. IR spectra in the amide I′ region of prion rods dispersed in detergent (A and B) and detergent–phospholipid mixed micelles (C–F). Prion rods (100 μg of protein) were dispersed in 100 μl of 10 mM phosphate buffer (pH 7.4) containing octyl β-D-glucopyranoside (spectrum A) or SDS (spectrum B) at 1 mg/ml. DLPCs were prepared by adding the protein–detergent (β-D-glucopyranoside) dispersion to a dried phospholipid film equivalent to 1 μg/μl. Phospholipids used were dimyristoyl DL-α-phosphatidylcholine (spectrum C), dioleoyl DL-α-phosphatidylcholine (spectrum D), dimyristoyl DL-α-phosphatidylglycerol (spectrum E), and dioleoyl DL-α-phosphatidylglycerol (spectrum F). Samples were incubated overnight and briefly sonicated three times during a 2-min period in a bath sonicator.

PrP 27-30 Secondary Structure Changes Upon Denaturation. Scrapie infectivity of prion rods has been shown to be diminished upon denaturation of PrP 27-30 by SDS (10). The complete absence of an amide II band after deuteration suggests that denatured PrP 27-30 purified by SDS/PAGE (Fig. 1, spectrum B) is far more accessible for hydrogen exchange and is less compact than when polymerized into prion rods, consistent with its increased solubility after denaturation. The amide I′ band after SDS/PAGE purification (Fig. 2*B*; Table 1, row C) revealed a major reduction in β-sheet content to the level predicted theoretically and a 3-fold increase in the turn content. The reduction in β-sheet is substantial for the LF β-sheet associated with intermolecular aggregation. The remaining absorption attributed to LF β-sheet maximizes at a very low frequency (1617 cm^{-1}), perhaps due to partial irreversible denaturation of PrP 27-30 from boiling in SDS, as bands at 1616 cm^{-1} are highly characteristic of thermally denatured proteins (30). The α-helix content is lower than predicted, but the increase in the turn content could arise from the formation of short or distorted helices (31), possibly due to the helicogenic effect of SDS. Broadening of the Lorentzian band at 1666 cm^{-1} due to turns lends support to this hypothesis.

Whether some of the spectral changes in PrP 27-30 following SDS/PAGE could result from the removal of non-PrP components from the prion rods remains to be established. However, ATR–FTIR spectra of PrP 27-30 treated with SDS revealed similar reductions in the β-sheet content. We have not quantitated these data, as the effects of SDS were more variable than other treatments, but the change in the amide I band is illustrated in Fig. 3, spectrum B. The similarity in the ATR–FTIR spectra for prion rods boiled in SDS and PrP 27-30 purified by SDS/PAGE argues that most, if not all, of the IR spectral features of the rods are due to PrP 27-30.

Alterations in PrP 27-30 Secondary Structure by Ionic Strength and pH. Increasing the salt concentration up to 0.25 M NaCl failed to induce any noticeable change in the amide I′ band, indicating no alteration overall in the secondary structure (data not shown). Higher ionic strengths decreased absorption efficiency, almost certainly due to poor interaction of the protein sample with the ATR element. The conformational stability of PrP 27-30 with varying salt concentrations argues for the involvement of multiple molecular

forces in the maintenance of amyloid polymers, a conclusion supported by studies of other amyloids (32).

In contrast to the stability of the ATR–FTIR spectrum of PrP 27-30 in salt, conformational transitions of PrP 27-30 were observed over the pH range 2–12 (Figs. 4 and 5; Table 1, rows D and E). The ratio A_{1630}/A_{1660}, corresponding to the spectral maximum and shoulder of the native state (Fig. 1, spectrum A), provided a relative measure of the β-sheet to α-helix content. This ratio was used to follow conformational transitions of PrP 27-30. Acidification produced a reversible transition that was accompanied by no change in prion solubility (Fig. 4), a decrease in β-sheet content, and an increase in random coil (Fig. 5; Table 1, row D). Earlier studies described the precipitation of the scrapie agent upon acid treatment without changes in infectivity (33).

Alkaline pH induced a spectral transition centered at pH 10 and an increase in solubility (Fig. 4). Analysis of the amide I band revealed increased helical content and a simultaneous decrease in β-sheet content although the intermolecular associations as shown by LF β-sheet were not strongly affected. A comparison of acid and alkali treatment (Table 1, row D vs. row E) showed that reversible changes induced by acid were less profound than the irreversible changes induced by alkali. Inactivation of prion infectivity, disassembly of the rods, and acquisition of protease sensitivity at pH 10 have been found (34); perhaps the irreversible alterations in the secondary structure of PrP 27-30 underlie these changes. Depolymerization of β/A4 peptide (amino acids 1–28) and a conformational change involving a β-sheet → α-helix transition have been reported to occur at pH 10 (32).

DISCUSSION

Since prions are composed largely, if not entirely, of PrP^{Sc}, we investigated the secondary structure of PrP 27-30 under conditions that perturb infectivity. Prion rods isolated by discontinuous sucrose gradient ultracentrifugation consist of 54% β-sheet, 25% α-helix, 10% turn, and 11% random coil. The LF β-sheet component that maximizes at 1621.5 cm^{-1} and accounts for one-third of the overall secondary structure presumably reflects the presence of intermolecular β-pleated sheets. The high content of LF β-sheet is consistent with the polymerization of PrP 27-30 into rod-shaped structures indistinguishable ultrastructurally and tinctorially from many purified amyloids (10). While prion rods are an artifact created during the purification of PrP^{Sc} (11), they reflect the ability of PrP^{Sc} to polymerize into amyloid within the brain (14). Immunocytochemical identification of human PrP within amyloid plaques has been extended by amino acid sequencing of the major component of the plaques, which is an 11-kDa PrP fragment (residues 58–150) (35) in the brains of patients dying from an inherited prion disease with a mutation at PrP codon 198 (36).

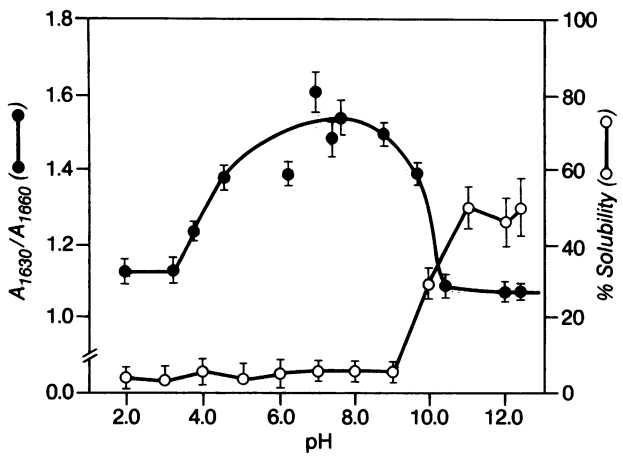

FIG. 4. pH-induced conformational transitions in PrP 27-30, shown by amide I′ absorption intensity ratio A_{1630}/A_{1660} (●) and solubility (○). Values represent the average (± SD). Samples were prepared in 10 mM phosphate buffers of different pH. Continuous titration was performed by adjusting the pH with suitable amounts of HCl and NaOH. The presence of nondenaturing detergent (β-D-glucopyranoside) gave analogous results.

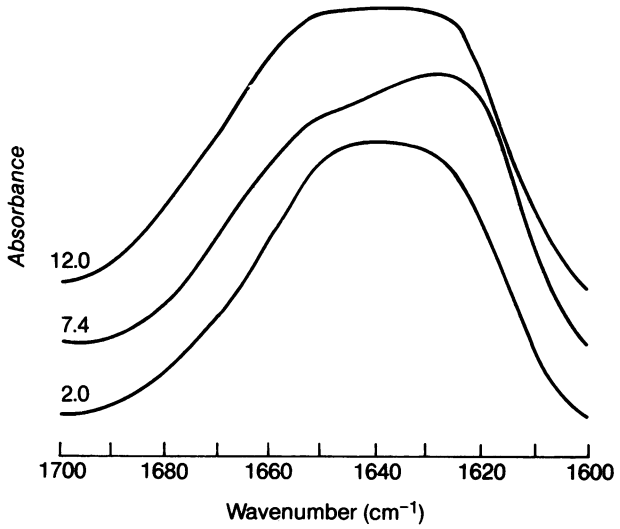

FIG. 5. Amide I′ absorption band for PrP 27-30 at pH 2.0, 7.4, and 12.0.

β-Sheet structures can be separated into two components, one maximizing at 1632 cm^{-1} and a lower-frequency component at 1621.5 cm^{-1}. For several proteins, the LF β-sheet component has been associated with the surface of lipid bilayers (37), and for others it has been ascribed to intermolecular β-sheet formation and aggregation (38). The latter is consistent with the amyloid properties of the prion rods and synthetic β/A4 peptides (32).

Variations of up to 8.5% between the secondary structure of proteins measured by ATR–FTIR and x-ray crystallography have been reported (20). In our study, spectral modifications were clearly visible in the original spectrum and thus were not artifacts of the deconvolution. Although PrP 27-30 is the major component of prion rods (10, 13), errors may arise due to minor copurifying substances such as oligonucleotides, glycosaminoglycans, and short peptides, which are likely to absorb in the amide I′ region. Adjustments for interfering absorbances that could be quantified proved not to be significant.

Heterogeneity in PrP 27-30 molecules can result from ragged N termini (39), truncation of the C terminus at Gly-228 rather than Ser-231 (27), and the resulting absence of the glycosylinositol phospholipid anchor in a significant fraction, as well as from variability in the Asn-linked oligosaccharides (24). Such sources of variation are not readily amenable to experimental manipulation, but size heterogeneity was minimized by isolation of a relatively uniform population of prion rods sedimenting in 48–60% sucrose in a discontinuous gradient. The composition, aggregate size, and specific infectivity were relatively constant and reproducible among different large-scale preparations (10).

Our results (Table 1, row A) differ in some respects from those of a transmission FTIR spectroscopy study of prion rods suspended in phosphate-buffered saline by sonication (β-sheet, 48%; α-helix, 14%; turn, 34%; coil, 4%; uncorrected for carbohydrate and side-chain contributions; ref. 21). While the β-sheet content was similar, the α-helix and coil contents

were lower and the turn content higher. Factors that could contribute to these discrepancies include differences in the IR technique, data analysis, sample pH, and purification protocols. Discontinuous sucrose gradient ultracentrifugation (10) appeared to give prion rods that were more homogeneous in size than those obtained by the differential ultracentrifugation protocol (40) used by Caughey *et al.* (21). Their scheme employed repeated sonication in the presence of high levels of detergent and salt—procedures that may denature or perturb the secondary structure of PrP 27-30. The discrepancies in the secondary structure may also be due to aggregation in the phosphate-buffered saline used for vigorous sonication of the prion rods just prior to obtaining transmission IR spectra (21).

Perturbations in the secondary structure of PrP 27-30 as measured by ATR–FTIR spectroscopy correlated well with changes in scrapie infectivity. Conditions that reduced β-structure were accompanied by disassembly of the prion rods and a diminution of infectivity. In contrast, disruption of the prion rods by dispersion into DLPCs occurred without a change in either PrP 27-30 secondary structure or prion infectivity. In some instances, scrapie infectivity has been shown to be 10- to 100-fold higher in DLPCs than in rods, presumably because of an increase in the efficiency of infection rather than an intrinsic change in PrP 27-30 structure (29, 41), a conclusion supported by the ATR–FTIR measurements.

Additional correlations of PrP 27-30 secondary structure and scrapie infectivity were obtained with acid, alkali, and SDS. At acidic pH, reversible changes in secondary structure were recorded under conditions that do not destroy infectivity, which could be of importance physiologically, whereas alkali produced an irreversible structural change and a loss of infectivity (33, 42). While phospholipids induced little structural change, SDS increased the α-helix and turn content at the expense of the β-sheet structure. The most profound alterations were associated with SDS/PAGE (10, 34) and, to a lesser extent, alkali treatment (33), both of which are known to destroy infectivity.

The results of the secondary structure studies reported here and by others (21) on nondenatured PrP 27-30 are consistent with earlier observations that demonstrated the polymerization of PrP 27-30 into amyloid (10). Secondary structural changes that appear to correlate with alterations in scrapie prion infectivity suggest that the conversion of PrP^{C} into PrP^{Sc} and the acquisition of infectivity are consequences of a structural transformation. Supporting this proposal are studies predicting that PrP^{C} might fold into a four-α-helix bundle (J.-M. Gabriel, F. Cohen, R.J.F., and S.B.P., unpublished work), whereas synthetic peptides corresponding to three of the four putative α-helices have a high β-sheet content and polymerize into amyloid (25). If the conversion of PrP^{C} into PrP^{Sc} and the replication of prions are consequences of a change in PrP structure, it will be of interest to look for other degenerative diseases that might prove to be disorders of protein conformation.

We thank Dr. Erik Goormaghtigh for the software and for his constant encouragement and helpful comments. We thank Dr. Joel White for providing access to the IR spectrophotometer and Fred Cohen for his review of the manuscript. Technical assistance was provided by A. Serban, R. Cotter, M. Elepano, Y. Zebarjadian, and D. Groth. M.G. was supported by a postdoctoral fellowship from the Consejo Superior de Investigaciones Cientificas, Spain. This work was supported by research grants from the National Institutes of Health (AG02132, NS14069, AG08967, and NS22786) and American Health Assistance Foundation and by gifts from the Sherman Fairchild Foundation, the Bernard Osher Foundation, and National Medical Enterprises.

1. Gajdusek, D. C. (1977) *Science* **197,** 943–960.
2. Prusiner, S. B. (1991) *Science* **252,** 1515–1522.
3. Borchelt, D. R., Scott, M., Taraboulos, A., Stahl, N. & Prusiner, S. B. (1990) *J. Cell Biol.* **110,** 743–752.
4. Caughey, B. & Raymond, G. J. (1991) *J. Biol. Chem.* **266,** 18217–18223.
5. Borchelt, D. R., Taraboulos, A. & Prusiner, S. B. (1992) *J. Biol. Chem.* **267,** 6188–6199.
6. Meyer, R. K., McKinley, M. P., Bowman, K. A., Braunfeld, M. B., Barry, R. A. & Prusiner, S. B. (1986) *Proc. Natl. Acad. Sci. USA* **83,** 2310–2314.
7. Kascsak, R. J., Rubenstein, R., Merz, P. A., Tonna-DeMasi, M., Fersko, R., Carp, R. I., Wisniewski, H. M. & Diringer, H. (1987) *J. Virol.* **61,** 3688–3693.
8. Serban, D., Taraboulos, A., DeArmond, S. J. & Prusiner, S. B. (1990) *Neurology* **40,** 110–117.
9. Stahl, N., Borchelt, D. R. & Prusiner, S. B. (1990) *Biochemistry* **29,** 5405–5412.
10. Prusiner, S. B., McKinley, M. P., Bowman, K. A., Bolton, D. C., Bendheim, P. E., Groth, D. F. & Glenner, G. G. (1983) *Cell* **35,** 349–358.
11. McKinley, M. P., Meyer, R., Kenaga, L., Rahbar, F., Cotter, R., Serban, A. & Prusiner, S. B. (1991) *J. Virol.* **65,** 1440–1449.
12. Bolton, D. C., McKinley, M. P. & Prusiner, S. B. (1982) *Science* **218,** 1309–1311.
13. Prusiner, S. B., Bolton, D. C., Groth, D. F., Bowman, K. A., Cochran, S. P. & McKinley, M. P. (1982) *Biochemistry* **21,** 6942–6950.
14. DeArmond, S. J., McKinley, M. P., Barry, R. A., Braunfeld, M. B., McColloch, J. R. & Prusiner, S. B. (1985) *Cell* **41,** 221–235.
15. Merz, P. A., Somerville, R. A., Wisniewski, H. M. & Iqbal, K. (1981) *Acta Neuropathol. (Berlin)* **54,** 63–74.
16. Diringer, H., Gelderblom, H., Hilmert, H., Ozel, M., Edelbluth, C. & Kimberlin, R. H. (1983) *Nature (London)* **306,** 476–478.
17. Glenner, G. G., Eanes, E. D., Bladen, H. A., Linke, R. P. & Termine, J. D. (1974) *J. Histochem. Cytochem.* **22,** 1141–1158.
18. Glenner, G. G. (1980) *N. Engl. J. Med.* **302,** 1283–1292.
19. Bazan, J. F., Fletterick, R. J., McKinley, M. P. & Prusiner, S. B. (1987) *Protein Eng.* **1,** 125–135.
20. Goormaghtigh, E., Cabiaux, V. & Ruysschaert, J.-M. (1990) *Eur. J. Biochem.* **193,** 409–420.
21. Caughey, B. W., Dong, A., Bhat, K. S., Ernst, D., Hayes, S. F. & Caughey, W. S. (1991) *Biochemistry* **30,** 7672–7680.
22. Garnier, J., Osguthorpe, D. J. & Robson, B. (1978) *J. Mol. Biol.* **120,** 97–120.
23. McKinley, M. P., Braunfeld, M. B., Bellinger, C. G. & Prusiner, S. B. (1986) *J. Infect. Dis.* **154,** 110–120.
24. Endo, T., Groth, D., Prusiner, S. B. & Kobata, A. (1989) *Biochemistry* **28,** 8380–8388.
25. Gasset, M., Baldwin, M. A., Lloyd, D., Gabriel, J.-M., Holtzman, D. M., Mobley, W. C., Cohen, F., Fletterick, R. & Prusiner, S. B. (1992) *Proc. Natl. Acad. Sci. USA*, in press.
26. Tarr, G. E. (1986) in *Methods of Protein Microcharacterization*, ed. Shively, J. E. (Humana, Clifton, NJ), pp. 154–194.
27. Stahl, N., Baldwin, M. A., Burlingame, A. L. & Prusiner, S. B. (1990) *Biochemistry* **29,** 8879–8884.
28. Chirdadze, Y. N., Fedorov, O. V. & Trushina, N. P. (1975) *Biopolymers* **14,** 679–694.
29. Gabizon, R., McKinley, M. P. & Prusiner, S. B. (1987) *Proc. Natl. Acad. Sci. USA* **84,** 4017–4021.
30. Surewicz, W. K., Leddy, J. J. & Mantsch, H. H. (1990) *Biochemistry* **29,** 8106–8111.
31. Kennedy, D. F., Crisma, M., Toniolo, C. & Chapman, D. (1991) *Biochemistry* **30,** 6541–6548.
32. Fraser, P. E., Nguyen, J. T., Surewicz, W. K. & Kirschner, D. A. (1991) *Biophys. J.* **60,** 1190–1201.
33. Prusiner, S. B., Groth, D. F., McKinley, M. P., Cochran, S. P., Bowman, K. A. & Kasper, K. C. (1981) *Proc. Natl. Acad. Sci. USA* **78,** 4606–4610.
34. Bolton, D. C., McKinley, M. P. & Prusiner, S. B. (1984) *Biochemistry* **23,** 5898–5906.
35. Tagliavini, F., Prelli, F., Ghisto, J., Bugiani, O., Serban, D., Prusiner, S. B., Farlow, M. R., Ghetti, B. & Frangione, B. (1991) *EMBO J.* **10,** 513–519.
36. Hsiao, K., Dloughy, S., Ghetti, B., Farlow, M., Cass, C., Da Costa, M., Conneally, M., Hodes, M. E. & Prusiner, S. B. (1992) *Nature Genet.* **1,** 68–71.
37. Cabiaux, V., Brasseur, R., Wattiez, R., Falmagne, P., Ruysschaert, J.-M. & Goormaghtigh, E. (1989) *J. Biol. Chem.* **264,** 4928–4938.
38. Jackson, M. & Mantsch, H. H. (1991) *Biochim. Biophys. Acta* **1078,** 231–235.
39. Prusiner, S. B., Groth, D. F., Bolton, D. C., Kent, S. B. & Hood, L. E. (1984) *Cell* **38,** 127–134.
40. Bolton, D. C., Bendheim, P. E., Marmorstein, A. D. & Potempska, A. (1987) *Arch. Biochem. Biophys.* **258,** 579–590.
41. Gabizon, R., McKinley, M. P., Groth, D. F., Kenaga, L. & Prusiner, S. B. (1988) *J. Biol. Chem.* **263,** 4950–4955.
42. Brown, P., Rohwer, R. G. & Gajdusek, D. C. (1984) *N. Engl. J. Med.* **310,** 727.